The Effects of Cell Sizes, Environmental Conditions, and Growth Phases on the Strength of Individual W303 Yeast Cells Inside ESEM

Mohd Ridzuan Ahmad*, *Student Member, IEEE*, Masahiro Nakajima, *Member, IEEE*, Seiji Kojima, Michio Homma, and Toshio Fukuda, *Fellow, IEEE*

***Abstract*—We performed in situ measurements of mechanical properties of individual W303 wild-type yeast cells by using an integrated environmental scanning electron microscope (ESEM)-nanomanipulator system. Compression experiments to penetrate the cell walls of single cells of different cell sizes (about 3–6 μm diameter), environmental conditions (600 Pa and 3 mPa), and growth phases (early log, mid log, late log and saturation) were conducted. The compression experiments were performed inside ESEM, embedded with a 7 DOF nanomanipulator with a sharp pyramidal end effector and a cooling stage, i.e., a temperature controller. ESEM itself can control the chamber pressure. Data clearly show an increment in penetration force, i.e., 96 $\pm$ 2, 124 $\pm$ 10, 163 $\pm$ 1, and 234 $\pm$ 14 nN at 3, 4, 5, and 6 μm cell diameters, respectively. Whereas, 20-fold increase in penetration forces was recorded at different environmental conditions for 5 μm cell diameter, i.e., 163 $\pm$ 1 nN and 2.95 $\pm$ 0.23 μN at 600 Pa (ESEM mode) and 3 mPa (HV mode), respectively. This was further confirmed from quantitative estimation of average cell rigidity through the Hertz model, i.e., ESEM mode (3.31 $\pm$ 0.11 MPa) and HV mode (26.02 $\pm$ 3.66 MPa) for 5 μm cell diameter. Finally, the penetration forces at different cell growth phases also show the increment pattern from log (early, mid, and late) to saturation phases, i.e., 161 $\pm$ 25, 216 $\pm$ 15, 255 $\pm$ 21, and 408 $\pm$ 41 nN, respectively.**

***Index Terms*—Cell mechanics, environmental-scanning electron microscope (SEM), nanomanipulation, single-cell analysis, yeast cells.**

I. Introduction

THE CONVENTIONAL approach to characterize cellular biology is called biochemistry. This developed science is used for studying physiological aspects, mainly genetics, by characterizing protein and other biomaterials. Since single cells are difficult to study, a collection of cells is used for characterizing cellular physiology and in turn used to describe the behavior of a single cell [1]. However, in addition to this advance understanding of cellular genetics, information about mechanical properties of cells is also needed. The molecular structure of the cell wall is only partially understood, and its mechanical properties are an area of "near-total darkness" [2]. Moreover, the approximation of single-cell behavior from a group used in conventional approach also requires further justification whether it can be applied to all cell types [3], [4]. This knowledge of cell mechanics could be valuable in future for biomedical applications, for example, variations in cell mechanics of healthy and unhealthy cells can be linked to a specific disease. In this paper, we show three kinds of cell mechanic characterization of a single yeast cell based on cell size, environmental conditions, and growth phases. This information can be used as a standard procedure for future disease detection.

Numerous methods such as micropipette aspiration, osmotic swelling/shrinking, cell poking, and cell compression [5] have enabled the response of the whole *Saccharomyces cerevisiae* cells to applied forces to be measured [6]; however, the mechanical properties of different cell sizes remain unknown. Recent advances in atomic force microscopy (AFM) have shown extensive research progress in the biomechanics of the living cells [7]–[9], however the effect of environmental conditions on these properties is still unknown. The mechanical characterization of yeast cells at log and saturation phases have been reported [6], but detailed mechanics at early, mid, and late log have not been investigated.

Therefore, we developed an integrated environmental scanning electron microscope (ESEM)-nanomanipulator system. Unlike the conventional SEM, ESEM enables soft, moist, and/or electrically insulating materials to be imaged without prior specimen preparation. A low-pressure (up to around 1333 Pa) gas can be accommodated around the sample. When this gas is water, hydrated samples can be maintained in their native state [10]. Sample temperature can be controlled by using the cooling stage assembled inside the ESEM chamber. By controlling the chamber pressure and sample temperature, single-cell mechanical characterization and analysis can be conducted by using a nanomanipulator and image analysis. By modifying a cantilever tip using focused ion beam (FIB) etching and/or deposition, several shapes of indenters for indenter–cell interactions can be applied. There are two main advantages of the ESEM system compared to the AFM system. The first advantage is that the AFM system is difficult to provide a real-time sample observation and the image is mainly constructed after the scanning of the AFM tip on the sample surface is finished. Therefore, it is

Manuscript received March 25, 2008; revised June 18, 2008. Current version published August 29, 2008. This work was supported in part by the Malaysian Government Scholarship under Grant UTM-SLAB and in part by the Ministry of Education, Culture, Sports, Science, and Technology (MEXT.KAKENHI). *Asterisk indicates corresponding author.*

*M. R. Ahmad is with the Department of Micro-Nano Systems Engineering, Nagoya University, Nagoya 464-8603, Japan (e-mail: ridzuan@robo.mein.nagoya-u.ac.jp).

M. Nakajima and T. Fukuda are with the Department of Micro-Nano Systems Engineering, Nagoya University, Nagoya 464-8603, Japan.

S. Kojima and M. Homma are with the Department of Biological Science, Graduate School of Science, Nagoya University, Nagoya 464-8602, Japan.

Color versions of one or more of the figures in this paper are available online at http://ieeexplore.org.

Digital Object Identifier 10.1109/TNB.2008.2002281

difficult, if not impossible, to directly observe the response of the object during the sample manipulation. On the other hand, the ESEM system provides real-time sample observation that can be obtained before, during, and after the manipulation. This real-time observation capability of the ESEM system has many advantages such as in analyzing the dynamic response of the sample and sample selection/sorting for certain properties like cell size become much easier. The mechanical characterization and analysis capabilities that can be done on the sample can also be enhanced.

The second advantage is related to the manipulation aspect. The AFM system can only provide 2-D manipulation, due to the difficulty of the real-time observation. Although 2-D manipulation can measure the stiffness property of the sample, it lacks in the flexibility of manipulation thus limiting the area of sample that can be analyzed. Unlike the AFM system, the ESEM-nanomanipulation system can provide both 2-D and 3-D manipulations on the sample, thus increasing the flexibility of the measurement such as the stiffness characterization in different areas of the sample like bottom surface can be realized.

The characterization of mechanical properties of the cell requires no interference from other external pressures or forces on the cell surface. These external forces such as the osmotic pressure may prevent investigation of the true mechanical properties of cell experimentally. The ESEM system can provide environmental conditions for the cells in their native state without any effect of the osmotic pressure. Cells can be sustained by releasing low pressure of H_2O molecule gas inside the ESEM chamber to provide high relative humidity (up to 100%). Therefore, the stiffness data obtained from this experimental setting show better representation of the mechanical properties of the cell. Our objective is to show the capability and effectiveness of the ESEM system for reliable mechanical stiffness measurement of biological samples. In the present study, we discuss an *in situ* characterization of the mechanical properties of the W303 yeast cells using ESEM-nanomanipulator under three different cases, i.e., cell sizes, environmental conditions, and cellular growth phases.

II. ESEM-Nanomanipulation System

Nanomanipulation is an effective strategy for the characterization of basic properties of individual nanoscale objects and to construct nanoscale devices quickly and effectively. We have constructed a hybrid nanorobotic manipulation system integrated with a transmission electron microscope (TEM)-nanorobotic manipulator (TEM manipulator) and a scanning electron microscope (SEM)-nanorobotic manipulator (SEM manipulator) [11]. This system allows effective sample preparation inside SEM with wide working area and many DOFs of manipulation. It has high-resolution measurement and evaluation of samples inside a TEM capability. The sample chambers of these electron microscopes are set under the high-vacuum (HV) condition to reduce the disturbance of electron beam for observation. To observe the water-containing samples, e.g., biocells, drying treatment processes are additionally needed. Hence, direct

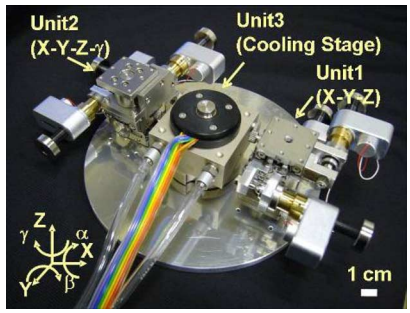

Fig. 1. Overview of the nanorobotic manipulator of the ESEM.

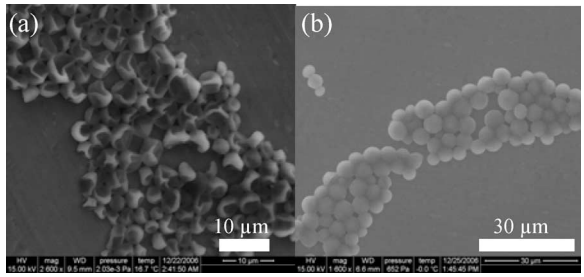

Fig. 2. Images of W303 yeast cells under. (a) HV mode. (b) ESEM mode.

observations of water-containing samples are normally quite difficult in these electron microscopes.

In the present study, we used the nanorobotic manipulators inside an ESEM [12]. It has been constructed with three units and 7 DOF in total (Fig. 1). The ESEM enables direct observation of water-containing samples with nanometer high resolution by a specially built secondly electron detector. The evaporation of water is controlled by both the sample temperature (0 °C–40 °C) and sample chamber pressure (10–2600 Pa). The temperature of the sample is controlled by the cooling stage unit (unit 3). The detail specifications of the manipulator and the ESEM can be obtained from our previous paper [13]. The following experiments have been conducted through this system.

III. ESEM Observation of Yeast Cells

The unique characteristic of the ESEM is the direct observation of the hydroscopic samples with nondrying treatment. Recently, the evaluation of biosamples has received much attention for nano-bio applications in nanobiotechnology. Since water is an important component for chemical reactions, nanomanipulation inside the ESEM could be a very effective tool for a water-containing sample with nanometer resolution.

Wild-type yeast cells (W303) were used for observation and measurements by the ESEM nanomanipulation system. The W303 cells were cultured on YPD plates (1% yeast extract, 2% peptone, 2% glucose, and 2% agar) in a 37 °C incubator for 24 h and dispersed in pure water. Several microliters of dispersed cells were placed on aluminum block on the cooling stage. The HV mode is operated at 16.7 °C and 3.03×10^{-3} Pa pressure. All yeast cells appeared concave and broken under HV mode. The ESEM mode is operated at 0 °C and ~600 Pa pressure and acceleration voltage is set at 15 kV. Under the ESEM mode, decreasing the pressure from ~700 Pa, water gradually evapo-

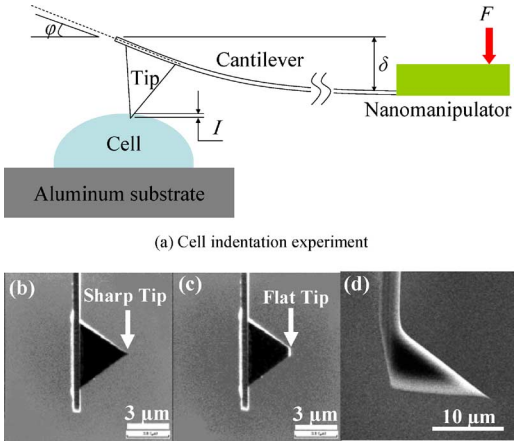

Fig. 3. Schematic diagram. (a) Indentation experiment. (b) Sharp. (c) Flat AFM pyramidal cantilever tips under the ESEM mode. For the HV mode. (d) Tetrahedral cantilever tip.

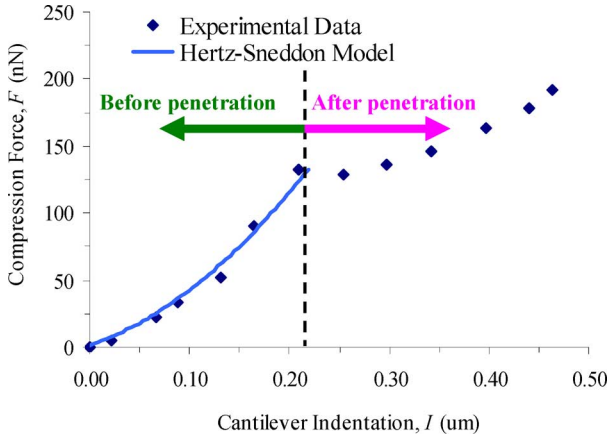

Fig. 4. Typical force—indentation (F–I) curve under ESEM mode using a sharp tip. The curve shows points before penetration (green arrow) and after penetration (pink arrow) of the cell. The blue line shows the best fit of the Hertz–Sneddon model of the experimental data until the penetration point (dotted line).

rates and the samples can be seen underneath. Their images are shown with HV and ESEM modes, as shown in Fig. 2(a) and (b). The remaining water can be seen at the intercellular spaces of yeast cells as black contrast [Fig. 2(b)]. Almost all yeast cells appear sphere shaped by water-contained condition under the ESEM operation.

IV. Mechanical Properties Characterization of Individual Yeast Cells

A. Determination of the Penetration Force and the Cell Stiffness

The indentation experiments [Fig. 3(a)] were conducted by using the integrated ESEM-nanomanipulation system. The cells were fixed on the cooling stage in perpendicular direction with an AFM cantilever (0.02 or 0.7 N/m spring constant). The AFM cantilever is controlled by the nanomanipulator and used to apply the compression force on each cell.

The penetration of a single cell by the AFM cantilever in this experiment was based on a direct observation of the cell when it was bursted by the AFM cantilever. Due to the shape and size of the indenters, i.e., pyramidal or tetrahedral tips (sharp or flat), the cell bursted phenomenon cannot be avoided as soon as the cell wall is penetrated [14].

The ESEM can provide real-time observation, i.e., a cell being approached, touched, indented, and finally, penetrated/bursted by the AFM cantilever can be seen clearly. Therefore, as far as this paper is concerned, the penetration of a single cell by the AFM cantilever was based on the occurrence of the cell bursting via real-time observation.

Force–cantilever indentation (F–I) curves were determined from the experiment. A typical F–I curve using a sharp cantilever tip shows a response of a cell before and after the penetration, as shown in Fig. 4. The value of F was calculated by using (1), where k, φ, and L are the spring constant, the displacement angle in radian, and the length of the cantilever, respectively. Values of φ, L, and I were determined from direct measurements of ESEM images using an image analysis software (ImageJ, developed at the National Institute of Health), while k was obtained from the manufacturer (Olympus Corporation). Equation (1) was derived from the Hooke's law, i.e., $F = k\delta$, where δ is the displacement of the cantilever that was obtained by using $\delta = \varphi(2/3)L$:

$$F = k\varphi\left(\frac{2}{3}\right)L \tag{1}$$

TABLE I
Values for Parameters Used in the Estimation of the Young's Modulus of the Single Cells

Parameters	Values
v	0.5
α	10°
R	20 nm
a	316 nm (ESEM mode) 206 nm (HV mode)

The Hertz–Sneddon models based on the shape of the tips, i.e., conical, spherical, and cylindrical, were used to estimate the Young's modulus of the cells, as expressed in (2)–(4). Parameters of E, v, α, R, and a are the Young's modulus, the Poisson's ratio ($v = 0.5$ for soft biological materials [15]) of the elastic half space (cell's surface), the half opening angle of a conical tip, the radius of curvature of a spherical tip and the radius of a cylindrical tip, respectively. Values for α, R, and a were obtained from ESEM images. Values for these parameters are summarized in Table I:

$$F_{\text{cone}} = \frac{2}{\pi}\tan\alpha\frac{E}{(1-v^2)}I^2 \tag{2}$$

$$F_{\text{spherical}} = \frac{4}{3}\frac{E}{(1-v^2)}R^{1/2}I^{3/2} \tag{3}$$

$$F_{\text{cylindrical}} = 2\frac{E}{(1-v^2)}aI \tag{4}$$

The models predict that the load depend on the indentation according to a power law related to the tip geometry [15]. In order to choose the correct tip geometry, an equation of the form

$F = mI^b$ was fitted to force versus indentation curves using commercial fitting software (DataFit), where the exponent b depends on the tip shape.

For the sharp pyramidal tip under ESEM mode, we obtained a value of b close to 3/2, characteristic of the spherical tip. The curves were then fitted by using the spherical model. Interestingly, under HV mode, the value of b close to 2 was obtained. Therefore, the canonical model was applied under HV mode. Finally, for the flat pyramidal tip, the b value close to 1 was obtained, which is for the cylindrical model. The fitting model for the sharp tip using the spherical tip was reported by Lanero *et al.* [15] while Touhami *et al.* [16] used the conical tip as their fitting equation. Obataya *et al.* [14] used the cylindrical equation to model their flat nanoneedles.

The Hertz–Sneddon models were derived from the classic Hertz's mechanics model for linear elastic material [17]. For flat cylindrical punch relating to an applied force F with an indentation depth I yields the following expression for the initial unloading (load is released after indentation) response, $dF/dI = cA^{1/2}(1-v^2)/E$, where c is coefficient [$c = 2/(\pi)^{1/2}$] and A is the contact area. The equation was based on the flat-ended punch, but holds true for any punch that can be described by a smooth solid revolution (spherical, conical, elliptical, etc.) [18]. Berkovich and Vickers indenters (three- and four-sided pyramidal cones, respectively) commonly applied in instrumented indentation techniques cannot be described as bodies of revolution. However, it has been found experimentally and by means of finite-element simulations that the deviation from the previous equation of pyramidal and other geometrical shapes is negligible [18]–[20]. The constant $c = 1.142$ for the pyramidal indenter and $c = 1.167$ for tetrahedral indenter differ little from $c = 2/(\pi)^{1/2} = 1.1284$ from the previous equation. In other words, the derived equation for the sharp conical tip can be used without large error, even the sharp indenter is not a true body of revolution.

The final equations of the Young's modulus based on the Hertz–Sneddon models, i.e., (2) and (3), and the parameter's values (Table I) for three different tip shapes, i.e., conical (HV mode), spherical (ESEM mode) and cylindrical (ESEM mode and HV mode), are expressed as

$$E_{\text{cell}} = (6.681)\frac{F_{\text{cone}}}{I^2} \tag{5}$$

$$E_{\text{cell}} = (3.977 \times 10^3)\frac{F_{\text{spherical}}}{I^{3/2}} \tag{6}$$

$$\begin{cases} E_{\text{cell}} = (1.187 \times 10^6)\dfrac{F_{\text{cylindrical}}}{I} & \text{(ESEM mode)} \\ E_{\text{cell}} = (1.825 \times 10^6)\dfrac{F_{\text{cylindrical}}}{I} & \text{(HV mode)} \end{cases} \tag{7}$$

Fig. 5 shows typical F–I curves using the spherical and cylindrical models under ESEM mode while the inset shows a curve using the conical model under HV mode as obtained in our experiments. The curves are shown until the bursting point of the cells, which is the maximum force which the cell can sustain before the cell is bursted. After the bursting point, the force will drop for a while due to the reversed force and will increase again when the tip traverses inside the cell or touches the bottom of the cell wall (Fig. 4). Starting from Fig. 5, data after the bursting points are not shown in the following figures. The reason for this exclusion is that the data were no longer representing the cell stiffness property since the cells were seriously damaged.

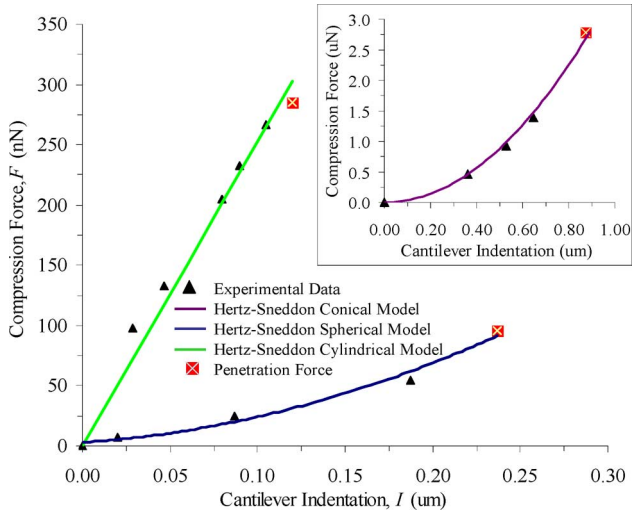

Fig. 5. Typical force—indentation (F–I) curves under ESEM mode using spherical and cylindrical models for sharp and flat tips, respectively. Inset shows the F–I curve under HV mode using conical model.

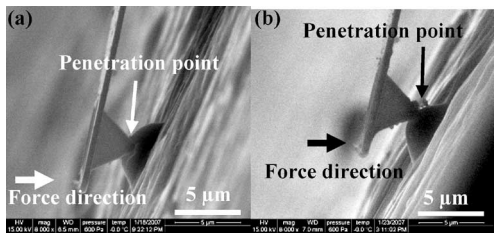

Fig. 6. Penetrations of yeast cells by different cantilever tips, i.e., (a) Sharp cantilever tip. (b) Flat cantilever tip.

The curve leading up to the failure is expected to give a combined elastic property of indenting the whole yeast cell and the localized deformation of the surface ruled by the properties of the cell-wall surface. Therefore, the reported E values in this paper indicate the maximum strength of the cell before bursting from a local indentation point. The E values must be higher than the local elastic cell property as the strength of the cell is dominated by the whole cell stiffness [6]. Nevertheless, examining the cell strength based on the Young's modulus parameter *per se* is not adequate since its value may remain constant at different situations, e.g., cell growth phases [6]. Therefore, the penetration force was used to determine the cell strength under several factors, i.e., cell sizes, environmental conditions, and cellular growth phases.

B. *Effect of Cell Sizes on the Strength of the Cells*

The penetrations of single yeast cells using sharp and flat cantilever tips [Fig. 3(b) and (c)] are shown in Fig. 6(a) and (b). The required force to penetrate a single yeast cell under the ESEM mode using a sharp tip for different cell sizes are

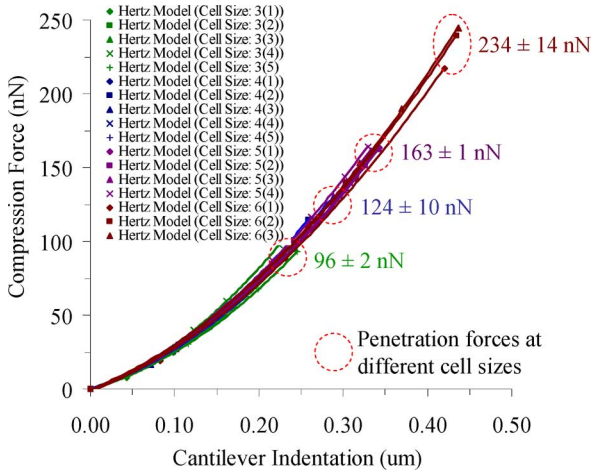

Fig. 7. Penetration force using a sharp tip at different cell sizes. Experimental data are fitted using the spherical model. The curves are shown until the penetration points. Inner bracket () indicates the cell number for each cell size. Cell size is in μm.

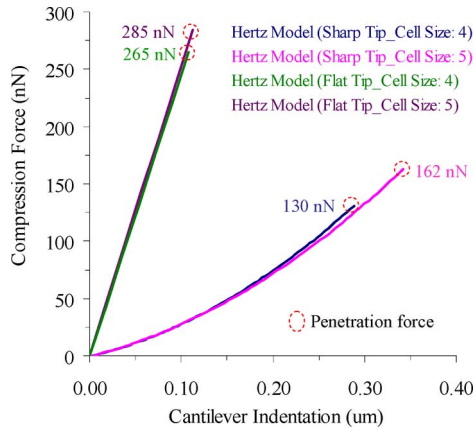

Fig. 8. Comparison of penetration force using sharp (using the spherical model) and flat tips (using the cylindrical model) for 4 and 5 μm cell sizes range. Young's modulus of the cells remains constant at about 3 MPa. The curves are shown until the penetration points.

shown in Fig. 7. The comparison between sharp and flat tips to penetrate each cell is shown in Fig. 8. The environmental settings for ESEM mode are set to 600 Pa and 0 °C. These parameters are chosen to vaporize water so that the majority of the cell surface can be seen for mechanical manipulation.

Results clearly show a strong relationship between the cell size and strength, the latter increases with an increase in the cell size (Fig. 7). Yeast cell walls consists predominantly of glucan with (1,3)-β and (1,6)-β linkages, and mannan covalently linked to protein (mannoprotein) [21]–[23]. Mechanical properties are a function of β-glucans, whereas mannoproteins control porosity [22], [24]. Thus, it can be inferred that the β-glucans composition increases when the yeast cell size increases. This prediction is consistent with other studies stating that small and large yeast cells exhibit similar glucan and mannan contents but further fractionation of the glucan showed five times less alkali-insoluble glucan in the smaller sized cells [25]. This may be another reason why the large yeast cells appear

TABLE II
YOUNG'S MODULUS OF THE SINGLE CELLS AT DIFFERENT CELL SIZES

Cell Size (μm)	Young Modulus (MPa)
~ 3	3.27 ± 0.23
~ 4	3.28 ± 0.12
~ 5	3.31 ± 0.11
~ 6	3.29 ± 0.10

to be stronger than the smaller cells [25]. The alkali-insoluble glucan plays a role in maintaining cell rigidity [26]. Nevertheless, the elastic properties of the cells at different sizes remain unchanged (Table II). The small and large yeast cells contain different composition levels of the alkali-insoluble glucan [25]. The increase in this glucan in the large cells does not change the properties of the molecule itself but rather increases the number of molecules, without changing its elasticity properties. Consequently, the elasticity of the whole cell also remains unchanged and independent of the cell size. On the other hand, since there are more glucan molecules in the larger cells, the thickness of the cell wall also increases [6]. Hence, the amount of force needed to penetrate the cell also increases due to more molecule barriers during the indentation that leads to penetration. The average penetration forces for 3, 4, 5, and 6 μm cell diameter ranges are 96 $\pm$ 2, 124 $\pm$ 10, 163 $\pm$ 1, and 234 $\pm$ 14 nN, respectively (Fig. 7). This was expected since the yeast's cell wall is remarkably thick (100–200 nm) [27], whereas its plasma membrane is only about 7 nm thick [27]. These results are comparable to reported penetration force of 1 nN for a human epidermal melanocytes that is the only cell membrane without cell wall structure [8]. Since the mechanical strength of the cell is provided by the cell wall and not the cell membrane, therefore, the melanocytes are easily penetrated compared to yeast cells. Additionally, the effect of local (small contact area between the tip and cell surface and global (large contact area between tip and cell surface) penetrations is also an important factor in the amount of applied force. This can be seen from our results for the local penetration (96–234 nN) compared to reported average of 149 $\pm$ 56 μN for global bursting of the yeast cell [6]. The average Young's modulus obtained from (6), i.e., 3.24 $\pm$ 0.09 MPa is reasonable compared to reported local cell stiffness values of 0.73 MPa [7] and 1.12 MPa [9], since the E values obtained in this paper represent not only the local elastic property of the cell but also the whole cell stiffness.

In addition to the cell size factor, we showed that the shape of the indenter also plays an important role in predicting the penetration force of a single cell. This can be confirmed from Fig. 8 where the penetration force can be reduced to 40%–50% by using a sharp cantilever tip compared to a flat tip. This provides a good indicator for future cell surgery where a minimal penetration force is required for preventing serious cell damage or undesirable mechanotransductions due to a large cell deformation [28]. The Young's modulus (E) of the cells estimated using the spherical model (sharp tip) and the cylindrical model

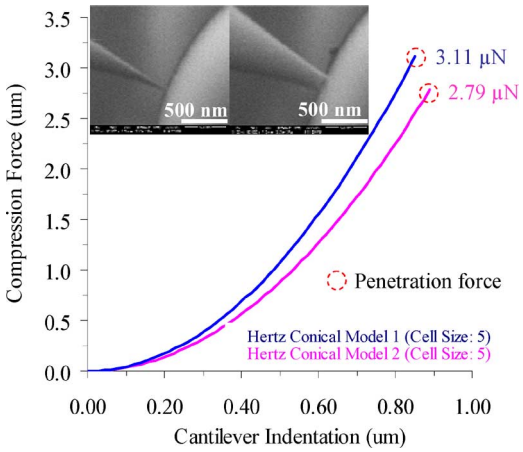

Fig. 9. Force-indentation curves until the penetration points using a sharp tip (conical model) for about 5 μm cell size under HV mode.

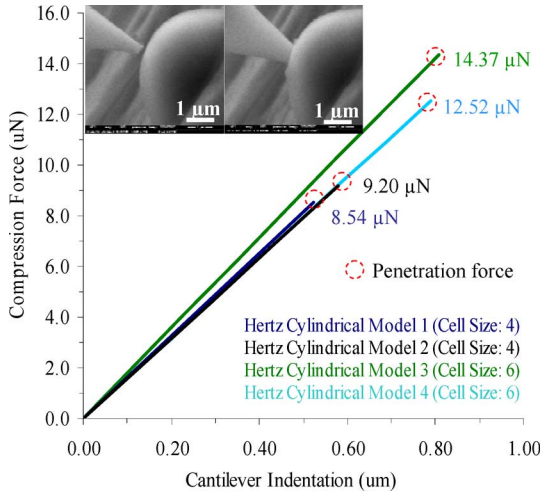

Fig. 10. Force-indentation curves until the penetration points using a flat tip (cylindrical model) for 4 to 6 μm cell sizes under HV mode.

(flat tip) obtained from (6) and (7), respectively, showed that the E values of the cell remained constant at about 3 MPa.

The link between the cell strength with the increase cell size as reported in this paper is somehow against the Laplace law. Laplace law governs the tension of an ideal thin-wall sphere, i.e., *Wall tension = Transmural pressure × Radius of the curvature* × $^1/_2$ [29]. From this equation, the more curved a membrane (small cell) is the less tension is experienced by the cell wall for a given transmural pressure (the pressure difference between inside and outside of the cell). The less is the tension the cell wall, the less is the possibility for the cell wall to fail. This means that smaller cell is less likely to be ruptured than a larger cell.

This notion could be true if the thickness of the cell remains constant independent of cell sizes. Since the cell wall plays a main role in cell stiffness than the membrane cell, any difference in the cell wall thickness would give different stiffness property of the cell. Smith *et al.* [6] showed that the thickness of the cell wall increases with the cell growth. Kliss *et al.* [21] also revealed that cells increase their size during their lifetime before undergoing a cell division. During this growing process, the composition of the β-glucan is increasing that, in turn, increases the thickness of the cell wall [6]. The heterogeneity of the cell wall composition and cell wall thickness will give different stiffness properties to the cell, and therefore, the Laplace law that governs the surface tension of the cell may play a minor role in predicting the strength of the cell.

C. Effect of the Environmental Conditions on the Strength of the Cells

The required force to penetrate a single yeast cell under HV mode using sharp and flat tips for different cell sizes are shown in Figs. 9 and 10, respectively. Insets are images of penetration of a single yeast cell using sharp (Fig. 9) and flat (Fig. 10) cantilever tips. Higher spring constant of the cantilever, i.e., 0.7 N/m was used for the compression experiment as lower spring constant values failed to penetrate the cell. Fig. 3(d) shows the image of a tetrahedral cantilever tip used in this experiment. The penetration force to burst a cell wall increases about 20 times from ESEM mode to HV condition (cells with 5 μm diameter were used for comparison and analysis) (Figs. 7 and 9). Since these data under HV condition are reported for the first time, it is difficult to compare with other reports. Nevertheless, the increase in penetration force from ESEM to HV modes that was obtained in our experiment can be logically understood. Cell wall construction is tightly controlled since polysaccharide composition, structure, and thickness of the cell wall vary considerably, depending on the environmental conditions [21]. Therefore, we can infer that under extreme condition of HV, the yeast cell tries to survive by increasing its wall thickness as suggested by the increased compression force needed to penetrate its cell wall (Figs. 9 and 10). Other possibility is that under HV condition, cells become too dry, which eventually increases their cell hardness. These findings reveal that besides the shape of a cantilever tip, other external factors such as environmental conditions also influence the penetration force of a single cell. Like the ESEM-mode, the cell size remains the internal factor that influences the penetration force under HV condition. By using a sharp tip, an average of 3 μN penetration force was required for a 5 μm diameter cell. As expected, this force increased (up to 14 μN) when a flat cantilever tip was applied, for cells with an average diameter of 4–6 μm.

TABLE III
YOUNG'S MODULUS OF THE SINGLE CELLS AT DIFFERENT ENVIRONMENTAL CONDITIONS

Environmental Conditions (Pa)	Young Modulus (MPa)
ESEM mode (~ 600)	3.31 ± 0.11 (n=4)
HV mode (~ 0.00314)	26.02 ± 3.66 (n=6)

For a quantitative evaluation of the elasticity of the cell, the Hertz–Sneddon mechanics model for conical and cylindrical tips, as expressed in (2) and (4), are used for sharp and flat tips, respectively. Average elastic properties of yeast cells under the influence of two environmental conditions are shown in

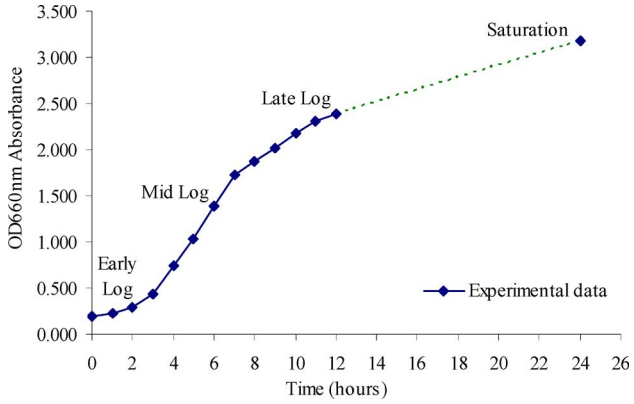

Fig. 11. Growth phase cycle for W303 yeast cells based on the $OD_{660\,nm}$ absorbance measurement.

Table III, where the cell stiffness increases about 10 times under the HV mode. The cell surface becomes rigid when it is placed in the HV mode. It is believed that in the absence of water, the cell surface becomes harder than in the presence of water. This leads to a significant increase in the Young's modulus (26.02 ± 3.66 MPa) obtained from (5) under the HV mode as compared to the ESEM mode (3.31 ± 011 MPa) as expected.

D. Effect of Growth Phases on the Strength of the Cells

All cells have a unique growth phase curve during their life cycle that is normally divided into four phases: lag, log, saturation, and death phases. In the present study, we did not investigate the death phase. These phases can be easily identified from the optical density (OD) absorbance–time curve (Fig. 11). Lag phase is located at the initial lower horizontal line where the cells adapt themselves to growth conditions and the cells mature and divide slowly. Log phase can be seen from an exponential line where the cells have started to divide and grow exponentially. The actual growth rate depends upon the growth conditions. Saturation phase resembles a final upper horizontal line where the growth rate slows and ceases mainly due to lack of nutrients in the medium. During the death phase, all of nutrients are exhausted and the cells die [30]. It is believed that the mechanics of the normal cells have different properties at each of the phases. In this section, the mechanical properties of W303 yeast cells at four different growth phases (early, mid, late log and saturation) are discussed.

Since each cell has a unique growth phase, we determined the growth phase of W303 yeast cells by measuring the absorbance at 660 nm using a spectrophotometer (Hitachi: U-2000) at 1 h intervals (Fig. 11). The growth rate (absorbance per hour) was about 0.23, as can be seen from the slope of the curve. Samples were stored at −80 °C (Sanyo: MDF-291AT) to hold its growth before the compression experiment.

The compression experiments were done at 6 h intervals starting at early log phase and ending at saturation phase. Penetration force was analyzed for each phase as shown in Fig. 12(a)–(d). As expected, the force needed to penetrate a single cell increased from early log to saturation phase (161 ± 25, 216 ± 15, 255 ± 21, and 408 ± 41 nN), whereas the elastic properties of the cells

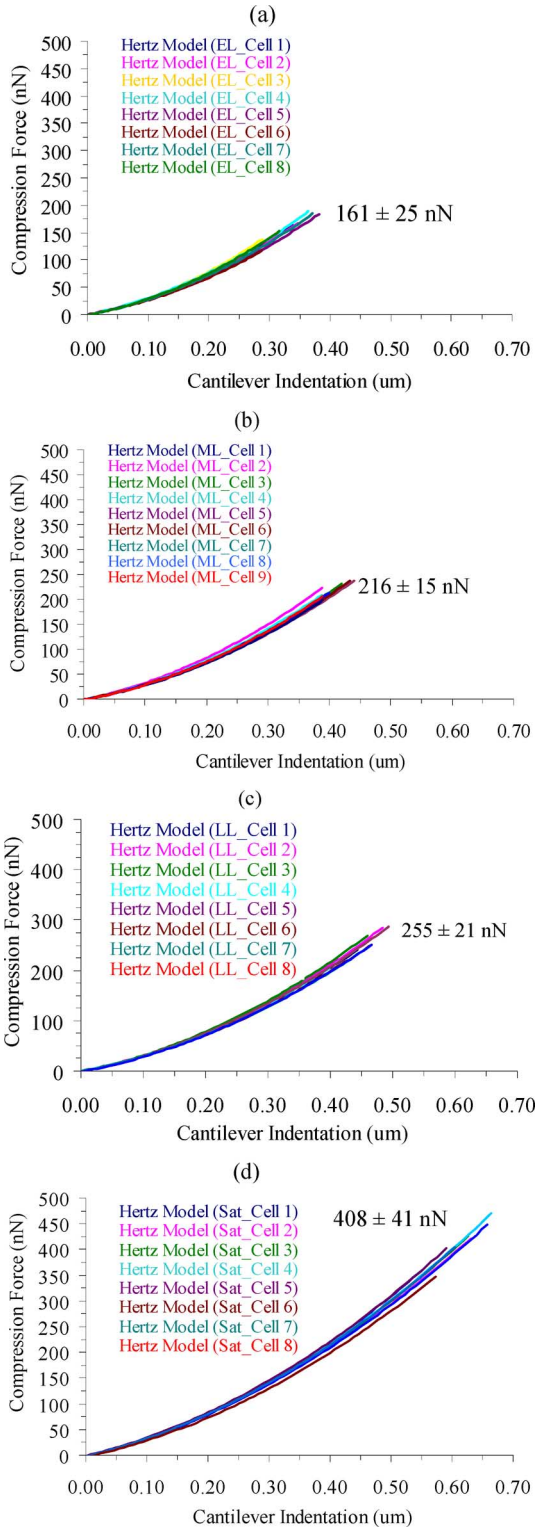

Fig. 12. Force-indentation curves (fitted using spherical model) for single cells at each growth phases. (a) Early log. (b) Mid log. (c) Late log. (d) Saturation. The curves are shown until the penetration points.

seem constant for all the phases obtained from (6), i.e., 3.28 ± 0.17, 3.34 ± 0.14, 3.24 ± 0.11, and 3.38 ± 0.11 MPa (Table IV). These mechanical properties of the W303 yeast cells at different growth phases are in an agreement with reported increment of average surface modulus of *Scerevisiae* cell wall to be 11.1 ± 0.6 N/m (log phase) and 12.9 ± 0.7 N/m (saturation phase) with

TABLE IV
YOUNG'S MODULUS OF THE SINGLE CELLS AT DIFFERENT CELL GROWTH PHASES

Cell Growth Phase	Young Modulus (MPa)
Early Log	3.28 ± 0.17 (n=8)
Mid Log	3.34 ± 0.14 (n=9)
Late Log	3.24 ± 0.11 (n=8)
Saturation	3.38 ± 0.11 (n=8)

no significant increase in the elastic modulus of the cell, i.e., 112 ± 6 MPa (log phase) and 107 ± 6 MPa (saturation phase) [6]. Their values for elastic modulus are quite high is also reasonable since they measured the whole elastic properties of the cell by compressing a single cell between two big flat indenters as compared to a local cell indentation in our case.

From this analysis, it can be inferred that the thickness of the W303 cell wall is increased during the growth phase since the penetration force increases at each phase, and at the same time, maintaining their elastic properties during the growth phase as verified by the constant elastic modulus values shown in Table IV. The increase in the cell thickness does not affect the elastic properties of the cell but the penetration force will be increased since more molecules need to be penetrated. We believe that the increase in the thickness of cell wall is mainly due to an increment of β-glucans molecules [22].

V. CONCLUSION

To the best of our knowledge, we, for the first time, have demonstrated the effect of the internal influences (cell size and growth phases) and the external influence (environmental conditions) on the cell strength. The penetration force is proportional to the increase in the cell size, during the cell growth and under HV condition. The elastic modulus of the cell increases dramatically under HV condition but remains unaffected during the cell growth. In the future, we are going to characterize the mechanics of diseased cells and these data can be compared to the mechanical properties of the normal cells, and eventually, some relation can be made between the cell mechanics and particular human disease. The advantage of the integrated ESEM-nanomanipulation system relies on its capability to perform *in situ* local direct observation and manipulation of biological samples and its ability to control environmental conditions.

ACKNOWLEDGMENT

The authors would like to thank Prof. Toshifumi Inada at Nagoya University for providing the yeast wild-type strain W303 cells.

REFERENCES

[1] B. F. Brehm-Stecher and E. A. Johson, "Single-cell microbiology: Tools, technologies, and applications," *Microbiol. Mol. Biol. Rev.*, vol. 68, pp. 538–559, 2004.
[2] F. M. Harold, "Molecules into cells: Specifying spatial architecture," *Microbiol. Mol. Biol.*, vol. 69, pp. 544–564, 2005.
[3] M. B. Elowitz, A. J. Levine, E. D. Siggia, and P. S. Swain, "Stochastic gene expression in a single cell," *Science*, vol. 297, pp. 1183–1186, 2002.
[4] H. M. Shapiro, "Microbial analysis at the single-cell level: Tasks and techniques," *J. Microbiol. Methods*, vol. 42, pp. 3–16, 2000.
[5] Y. C. Fung, *Biomechanics: Mechanical Properties of Living Tissue*, 2nd ed. New York: Springer-Verlag, 2005.
[6] A. E. Smith, Z. Zhang, C. R. Thomas, K. E. Moxham, and A. P. J. Middelberg, "The mechanical properties of *Saccharomyces cerevisiae*," *Proc. Nat. Acad. Sci.*, vol. 97, pp. 9871–9874, 2000.
[7] A. E. Pelling, S. Sehati, E. B. Gralla, J. S. Valentine, and J. K. Gimzewski, "Local nanomechanical motion of the cell wall of *Saccharomyces cerevisiae*," *Science*, vol. 305, pp. 1147–1150, 2004.
[8] I. Obataya, "Nanoscale operation of a living cell using an atomic force microscope with a nanoneedle," *Nano Lett.*, vol. 5, pp. 27–30, 2005.
[9] T. S. Lanero, "Mechanical properties of single living cells encapsulated in polyelectrolyte matrixes," *J. Biotechnol.*, vol. 124, pp. 723–731, 2006.
[10] A. M. Donald, "The use of environmental scanning electron microscopy for imaging wet and insulating materials," *Nat. Mater.*, vol. 2, pp. 511–516, 2003.
[11] M. Nakajima, F. Arai, and T. Fukuda, "*In situ* measurement of Young's modulus of carbon nanotube inside TEM through hybrid nanorobotic manipulation system," *IEEE Trans. Nanotechnol.*, vol. 5, no. 3, pp. 243–248, May 2006.
[12] M. Nakajima, F. Arai, and T. Fukuda, "Nanofixation with low melting metal based on nanorobotic manipulation," in *Proc. 6th IEEE Conf. Nanotechnol. (IEEE Nano 2006)*, pp. 925–928.
[13] M. R. Ahmad, M. Nakajima, S. Kojima, M. Homma, and T. Fukuda, "*In situ* single cell mechanical characterization of W303 yeast cells inside environmental-SEM," in *Proc. 7th IEEE Int. Conf. Nanotechnol.*, Hong Kong, 2007, pp. 1022–1027.
[14] I. Obataya, C. Nakamura, S. W. Han, N. Nakamura, and J. Miyake, "Nanoscale operation of a living cell using an atomic force microscope with a nanoneedle," *Nano Lett.*, vol. 5, pp. 27–30, 2005.
[15] T. S. Lanero, O. Cavalleri, S. Krol, R. Rolandi, and A. Gliozzi, "Mechanical properties of single living cells encapsulated in polyelectrolyte matrixes," *J. Biotechnol.*, vol. 124, pp. 723–731, 2006.
[16] A. Touhami, B. Nysten, and Y. F. Dufrene, "Nanoscale mapping of the elasticity of microbial cells by atomic force microscopy," *Langmuir*, vol. 19, pp. 4539–4543, 2003.
[17] I. N. Sneddon, "The relation between load and penetration in the axisymmetric boussinesq problem for a punch of arbitrary profile," *Int. J. Eng. Sci.*, vol. 3, pp. 47–57, 1965.
[18] G. M. Pharr, W. C. Oliver, and F. R. Brotzen, "On the generality of the relationship among contact stiffness, contact area, and elastic modulus during indentation," *J. Mater. Res.*, vol. 7, pp. 619–617, 2002.
[19] R. B. King, "Elastic analysis of some punch problems for a layered medium," *Int. J. Solids Struct.*, vol. 23, pp. 1657–1664, 1987.
[20] M. Dao, N. Chollacoop, K. J. Van Vliet, T. A. Venkatesh, and S. Suresh, "Computational modelling of the forward and reverse problems in instrumented sharp indentation," *Acta Mater.*, vol. 49, pp. 3899–3918, 2001.
[21] F. M. Klis, A. Boorsma, and P. W. J. D. Groot, "Cell wall construction in *Saccharomyces cerevisiae*," *Yeast*, vol. 23, pp. 185–202, 2006.
[22] G. Lesage and H. Bussey, "Cell wall assembly in *Saccharomyces cerevisiae*," *Microbiol. Mol. Biol. Rev.*, vol. 70, pp. 317–343, 2006.
[23] P. N. Lipke and R. Ovalle, "Cell wall architecture in yeast: New sturcture and new challenges," *J. Bacteriol.*, vol. 180, pp. 3735–3740, 1998.
[24] H. Zlotnik, M. P. Fernandes, B. Bowers, and E. Cabib, "*Saccharomyces cerevisiae* mannoproteins form an external cell wall layer that determines wall porosity," *J. Bacteriol.*, vol. 159, pp. 1018–1026, 1984.
[25] T. Srinorakutara, "Study on the effect of diluent osmotic pressure on yeast cell strength and cell size using a novel micromanipulation technique," *Int. J. Microbiol. Biotechnol.*, vol. 14, pp. 719–725, 1998.
[26] G. H. Fleet and D. J. Manners, "Isolation and composition of an alkali-soluble glucan from the cell walls of *Saccharomyces cerevisiae*," *J. Gen. Microbiol.*, vol. 94, pp. 180–192, 1976.
[27] G. M. Walker, *Yeast Physiology and Biotechnology*. Chichester, U.K.: Wiley, 1998.
[28] H. Huang, R. D. Kamm, and R. T. Lee, "Cell mechanics and mechanotransduction: Pathway, probes, and physiology," *Amer. J. Physiol. Cell Physiol.*, vol. 287, pp. C1–C11, 2004.
[29] C. E. Morris and U. Homann, "Cell surface area regulation and membrane tension," *J. Membr. Biol.*, vol. 179, pp. 79–102, 2000.
[30] G. J. Tortora, B. R. Funke, and C. L. Case, *Microbiology: An Introduction*, 8th ed. Redwood City, CA: Benjamin Cummings, 2003.

Mohd Ridzuan Ahmad (S'07) received the B.S. and M.S. degrees in electrical engineering from the Universiti Teknologi Malaysia (UTM), Skudai, Malaysia, in 2000 and 2004, respectively. He is currently working toward the Ph.D. degree in the Department of Micro-Nano Systems Engineering, Nagoya University, Nagoya, Japan.

From May 2000 to December 2001, he received a National Science Fellowship from the Ministry of Science, Technology, and Environment, Malaysia. From June to November 2002, he was a Research Officer in the Department of Robotics and Mechatronics, UTM. Since 2003, he has been a Lecturer in the Faculty of Electrical Engineering, UTM. He is also involved in robotics research field especially in multiagent robotics system. His current research interests include micro/nanomanipulation, nanobiology, biomechanics, and nanodevices.

Masahiro Nakajima (M'03) received the B.S. degree in mechanical engineering from Shizuoka University, Shizuoka, Japan, in 2001, and the M.S. and Dr. Eng. degrees in mechanical engineering from Nagoya University, Nagoya, Japan, in 2003 and 2006, respectively.

From April to May 2006, he was a Research Fellow in the Ministry of Education, Culture, Sports, Science, and Technology (MEXT), Nagoya University, where he was also a Research Associate from June 2006 to March 2007. Since April 2007, he has been an Assistant Professor in the Department of Micro-Nano Systems Engineering, Nagoya University. His current research interests include micro/nanomanipulation, nanoassembly, nanofabrication, nanodevices, nanomechanics, and nanobiology.

Seiji Kojima received the B.S., M.S. and Ph.D. degrees in biological sciences from Nagoya University, Nagoya, Japan, in 1994, 1996, and 1999, respectively.

From April 1999 to February 2004, he was a Postdoctoral Fellow in the Department of Biology, University of Utah, USA. From March 2004 to September 2005, he was a Postdoctoral Fellow at the Dynamic Nanomachine Project, ICORP JST, Japan. Since October 2005, he has been a Research Assistant Professor in the Department of Biological Science, Nagoya University. His current research interests include bacterial physiology, protein chemistry and structure, and visualization of protein behavior by fluorescent probes especially membrane proteins involved in energy conversion.

Michio Homma received the B.S. degree in biology from International Christian University, Tokyo, Japan, in 1980, and the M.S. and Dr. Science degrees in biology from Tokyo University, Tokyo, in 1982 and 1985, respectively.

From 1985 to 1992, he was a Postdoctoral Associate in the Department of Molecular Biophysics Biochemistry, Yale University. From 1988 to 1992, he was a Lecturer in the Research Institute for Disease Mechanism and Control, School of Medicine, Nagoya University, Nagoya, Japan. From 1992 to 1998, he was with the Department of Molecular Biology, Faculty of Science, Nagoya University. He has been a Professor in the Department of Biological Science, Graduate School of Science, Nagoya University. His current research interests include energy transduction and sensory transduction in bacteria.

Toshio Fukuda (M'83–SM'93–F'95) received the B. S. degree from Waseda University, Tokyo, Japan, in 1971, and the M.S. and Dr. Eng. degrees from the University of Tokyo, Tokyo, Japan, in 1973 and 1977, respectively.

From 1977 to 1982, he was with the National Mechanical Engineering Laboratory, Tsukuba, Japan. From 1982 to 1989, he was with the Science University of Tokyo, Tokyo. Since 1989, he has been with Nagoya University, Nagoya, Japan, where he is currently a Professor in the Department of Micro-Nano Systems Engineering. His current research interests include intelligent robotic systems, cellular robotic systems, mechatronics, and micronanorobotics.

Prof. Fukuda was the President of the IEEE Robotics and Automation Society during 1998–1999, the Editor-in-Chief of IEEE/ASME TRANSACTIONS ON MECHATRONICS during 2000–2002, the Director of the IEEE Division X, Systems and Control during 2001–2002, and the President of the IEEE Nanotechnology Council during 2002–2005.